PCCP
Physical Chemistry Chemical Physics

Accepted Manuscript

This article can be cited before page numbers have been issued, to do this please use: F. D. Villarruel, M. P. Denofrio, E. Wolcan , R. Erra-Balsells, F. S. García Einschlag, T. Schmidt De Leon and F. M. Cabrerizo, *Phys. Chem. Chem. Phys.*, 2024, DOI: 10.1039/D3CP05223K.

Exploring Photooxidative Degradation Pathways of Harmol and Harmalol alkaloids in Water: Effects of pH, Excitation Sources and Atmospheric Conditions

View Article Online
DOI: 10.1039/D3CP05223K

*Fernando D. Villarruel,[a] M. Paula Denofrio,[a] Tobías Schmidt de León,[b,c] Rosa Erra-Balsells,[b,c] Ezequiel Wolcan,[d] Fernando S. García Einschlag,[d] and Franco M. Cabrerizo[a,] **

[a] Instituto Tecnológico de Chascomús (INTECH), Universidad Nacional de San Martín (UNSAM) - Consejo Nacional de Investigaciones Científicas y Técnicas (CONICET), Av. Intendente Marino Km 8.2, CC 164 (B7130IWA), Chascomús, Argentina. E-mail: fcabrerizo@intech.gov.ar

[b] Universidad de Buenos Aires. Facultad de Ciencias Exactas y Naturales. Departamento de Química Orgánica. Pabellón II, 3er P., Ciudad Universitaria, (1428) Buenos Aires, Argentina.

[c] CONICET, Universidad de Buenos Aires. Centro de Investigación en Hidratos de Carbono (CIHIDECAR). Facultad de Ciencias Exactas y Naturales. Pabellón II, 3er P., Ciudad Universitaria, (1428) Buenos Aires, Argentina.

[d] Instituto de Investigaciones Fisicoquímicas Teóricas y Aplicadas (INIFTA), CCT-La Plata-CONICET, Universidad Nacional de La Plata, Diag. 113 y 64 (1900), La Plata, Argentina

* To whom correspondence should be addressed (fcabrerizo@intech.gov.ar)

ABSTRACT

This work explores the photochemical degradation of the cationic species of 7-hydroxy-1-methyl-2H-pyrido [3,4-b]indole or harmol (**1C**) and the corresponding partially hydrogenated derivative 7-hydroxy-1-methyl-3,4-dihydro-2H-pyrido [3,4-b]indole or harmalol (**2C**) in aqueous solution. UV–visible absorption and fluorescence emission spectroscopy coupled with multivariate data analysis (MCR-ALS and PARAFAC), HPLC and HRESI-MS techniques were used for both quantitative and qualitative analysis. The formation of hydrogen peroxide reactive oxygen species (ROS) was

quantified, and the influence of pH, oxygen partial pressure and photoexcitation source on the photochemical degradation of both compounds was assessed. The potential implications on the βCs biosynthesis and their biological role in living systems is discussed.

View Article Online
DOI: 10.1039/D3CP05223K

Keywords: β-carboline, alkaloids, photochemistry, PARAFAC, MCR-ALS

INTRODUCTION

β-carboline (βC) are heterocycle alkaloids found in various biological systems.[1–6] The biosynthesis of βCs involves an enzymatic Pictet-Sprengler condensation between tryptophan and aldehydes, leading to the formation of 1,2,3,4-tetrahydro- and 3,4-dihydro-βC derivatives. Subsequent chemical/enzymatic reactions may yield diverse βCs, including the full aromatic derivatives.[7] In addition, oxygen-dependent photoinduced oxidations and/or full aromatization can also play a role as it was demonstrated *in vitro* for harmaline, a related 3,4-dihydro-derivative.[8]

Among them, 7-hydroxy-1-methyl-9H-pyrido[3,4-b]indole, Harmol (**1**) and the corresponding 3,4-dihydro-derivative, Harmalol (**2**) (**Scheme 1**), are prominent constituents of the *Peganum harmala* seed extracts [9] and floral nectar. [10] Additionally, compounds **1** and **2** were found in *Passiflora caerulea* floral organs (*i.e.*, anthers, corona, stigmas, petals and sepals) [6], and their role in pollinator discrimination was hypothesized. [6,10]

From the pharmacological and biochemical viewpoints, these compounds have shown to be promising pharmaceutical drugs. [11,12] These alkaloids show antitumor, [13,14] antimicrobial, [15–18] cell growth inhibitory,[12] and *in vivo* and *in vitro* antioxidant [19–21] properties, among many others. Moreover, the use of compound **2** on hypopigmentation disorders treatment has been recently proposed due to its demonstrated capability to induce melanogenesis.[22]

In this context, understanding their photochemical properties becomes crucial. The photophysical properties of compound **2** in organic solvents have been previously studied,[23–25] and theoretical spectra predictions have also been reported.[26,27] Research of the photophysical properties of compounds **1** and **2** in aqueous environments were conducted very recently, combining spectroscopic studies, TD-DFT [28] and chemometrics approach. In particular, Parallel Factor Analysis (PARAFAC) and Multivariate Curve Resolution by Alternating Least Squares (MCR-ALS) were used for a deep understanding of these complex photoactive alkaloids.[8,29–31] Interestingly, multivariate analysis of spectroscopic data played a key role on the characterization of harmaline photoproducts (PPs).[8]

In this work, we report a photochemical study of the cationic (**C**) species of compounds **1** and **2**, in aqueous solution. The analysis of the photochemical reactions was carried out using UV-visible and fluorescence spectroscopies combined with chemometric analysis, HPLC chromatography, and HRESI-MS mass spectrometry. The effect of different experimental parameters including pH, irradiation wavelength, and oxygen partial pressure on the studied reactions was investigated.

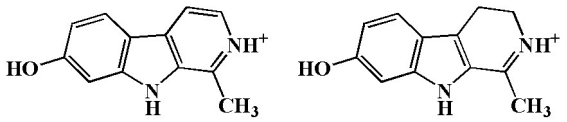

Harmol (**1C**) Harmalol (**2C**)

Scheme 1. Chemical structures of the cationic (**C**) species of compounds **1** y **2** studied in the present work.

EXPERIMENTAL

General

Chemicals: harmol and harmalol (> 98%, Sigma-Aldrich) were used without further purification. Catalase extract (C1345, Sigma-Aldrich) provided by the supplier was further purified. Briefly, the enzyme extract was dissolved/suspended, at a concentration of 30 U μl^{-1}, in water. It was then centrifugated at 10.000 rpm for 10 min and supernatant was extracted.

pH adjustment: The pH of βCs aqueous solutions was adjusted by adding drops of aqueous NaOH or HCl solutions from a micropipette. The concentrations of the acid and/or base solutions used for this purpose ranged from 0.1 to 2 M. The ionic strength was approximately 10^{-3} M in all the experiments.

Instrumentation and approaches for steady-state experiments.

Elapsed irradiation. βC´s aqueous solutions were irradiated in 1 cm quartz placed in a temperature-controlled cuvette holder (set at 25°C). Two different excitation sources were used: *(i)* UVA Rayonet RPR lamp (Southern N.E. Ultraviolet Co.) with its emission band centered at 350 nm and a half peak bandwidth of ± 15 nm (R-350), and *(ii)* A light-emitting diode with its emission band centered at 426 nm and a half peak bandwidth of ± 8 (LED-426) (**Figure SI.3**). Incident photon fluxes (P_0) for R-350 and LED-426 were 7.0×10^{-5} and 7.6×10^{-3} Einstein L^{-1} min^{-1}, respectively. Experiments were performed under air-equilibrated and under N_2-saturated (N_2-sat) atmosphere. The latter oxygen-free solutions were obtained by bubbling with N_2(5.0) gas for 20 min.

Spectroscopic analysis. Electronic absorption spectra were recorded on a Perkin-Elmer lambda 25 spectrophotometer,[32] whereas steady-state fluorescence measurements were performed using a Fluoromax4 (HORIBA Jobin Yvon) described elsewhere.[30]

High-Performance Liquid Chromatography (HPLC). A Waters 600E Pump Controller with a fluorescence detector was used to monitor and quantify the photochemical reactions. Aqueous solutions of commercial standards were employed for the calibration curves. A Supelco-C18 column (250 × 4.6 mm, 5 mm) was used for product separation, the elution being achieved with

a solution of 50% MeOH (J. T. Baker) and 50% formic acid (0.08% v/v) aqueous solution (pH 3.5), at an isocratic flux of 1 ml min^{-1}. The monitoring parameters were: $\lambda_{exc}/\lambda_{em}$ = 320 nm/420 nm and 370 nm/480 nm, to detect the signals corresponding to **1C** and **2C**, respectively.

Quantum yield determinations. The quantum yields of reactant disappearance (Φ_R) were obtained using the procedure described in the literature. [33]

Detection and quantification of H_2O_2. To this aim, a modified version of the methodology reported elsewhere [8,34] was implemented. Briefly, H_2O_2 produced upon irradiation was quantified by using the Glycemia enzymatic test (Wiener Lab.) that catalyse the reaction between H_2O_2 with 4-aminophenazone (AP) and phenol (PH). Aliquotes (0.5 mL) of irradiated (R-350) solution at different times were mixed with 0.6 mL of the colorimetric reagents AP and PH. The mixture was incubated during 40 min at room temperature and, after that, the absorbance at 505 nm (A^{505nm}) was measured. Calibration curve was obtained from aqueous H_2O_2 solutions prepared from commercial standards and the corresponding [H_2O_2] in each of the standard solutions was determined using a molar absorption coefficient at 254 nm (ε^{H2O2}) of 17.7 M^{-1} cm^{-1}. To avoid any potential interference from the βCs' photoproducts (PPs) that usually show non-negligible absorption coefficients at ~500 nm, a parallel set of irradiated solutions were incubated with 40 µL of purified catalase (30 U μL^{-1}) prior the incubation with the colorimetric reagents AP and PH for H_2O_2 determination. The comparison of the latter control experiments with data obtained in the absence of catalase (incubated with 40 µL of mili-Q water) allowed us to univocally establish whether the the signal observed at A^{505nm} is due to the H_2O_2 or due to interferences.

Parallel Factor Analysis (PARAFAC). PARAFAC analysis was conducted following the methodology described elsewhere.[8]

Computational methods. Computer calculations were performed following the methodology described elsewhere.[28,35] Briefly, the electronic structures of βCs were determined using tools of Density Functional Theory (DFT) as implemented in the Gaussian 09 package. The vacuum geometries were optimized at the B3LYP/TZVP level of theory. Vibrational frequencies were computed at the same level of theory to confirm that these structures were minima on the energy surfaces. The vertical transition energies were calculated at the optimized ground-state geometry by Time-Dependent-Density Functional Theory (TD-DFT) using a B3LYP hybrid functional and aug-cc-pVDZ basis set including solvent effects (water) through the Polarizable Continuum Model. Absorption spectra were simulated with Gaussian distributions with a full-width at half-maximum (fwhm) set to 3000 cm^{-1} with the aid of GaussSum 2.2.5 program.

RESULTS

Photochemistry of 1C and 2C in aqueous media

The photostability of compounds **1** and **2** in aqueous solution was studied under steady-state irradiation (i.e., R-350 and LED-426) in the pH range 4 - 7. The latter pH conditions allow to investigate those biologically relevant species. It is worth mentioning that, in the pH range 4-10, both compounds present one acid-base equilibria with pK_a values of 7.8 and 8.5, for **1** and **2**, respectively. Thus, under physiological pH (~7.2) the fraction of the cationic species **2C** is higher than 99%. [28] In the case of compound **1**, although a mixture of both neutral (**N**) and cationic (**C**) species is present under this pH condition, it was demonstrated that upon photoexcitation the dominant species is **1C***, due to the enhanced basicity shown by all the full aromatic βCs in their excited states. [28] The role of oxygen was monitored by performing the reactions under two different atmospheric conditions, *i.e.*, in air-equilibrated (air) and in N_2-saturated (N_2-sat) aqueous solutions.

Chromatographic analysis (HPLC)

The evolution of **1C** and **2C** concentrations as a function of irradiation time was evaluated first by HPLC chromatography. Samples were irradiated with the UVA lamp R-350 under acidic conditions (pH 4.2), in both atmospheres studied (air and N_2-sat). Under air-equilibrated aqueous solutions, both compounds showed photochemical degradation with pseudo-zero order kinetics in the time range analyzed, the consumption rates being 2.7 and 1.0 μM min^{-1} for compounds **1C** and **2C**, respectively (**Figure 1**). On the contrary, under N_2-sat atmosphere, these two compounds exhibited distinctive behavior. Briefly, compound **1C** is photostable whereas compound **2C** showed a pseudo-zero order kinetic of consumption with a rate of 0.6 μM min^{-1}. The corresponding quantum yields of disappearance (Φ_R), calculated considering the incident photon flux obtained by performing the corresponding actinometry, are depicted in **Table 1**. Interestingly, Φ_R values obtained for **1** and **2** (Φ_R ~ 10^{-2}) are 10-20-folds the Φ_R reported for other βCs (Φ_R ~ 10^{-3}-10^{-4}). [32,33,36] Thus, the presence of the hydroxyl group at C(7) in the βC ring may decrease the photostability of these alkaloids and/or may provide additional photodegradation pathways.

Table 1. Quantum yields of βC disappearance (Φ_R), measured in acidic (pH 4.2) air-equilibrated and N_2-sat aqueous solutions. R-350 was used as excitation source.

	1C	**2C**
Φ_R^{air}	83.0 (± 0.8) x 10^{-3}	20.3 (± 0.9) x 10^{-3}
$\Phi_R^{N2\text{-}sat}$	0	11.6 (± 0.5) x 10^{-3}

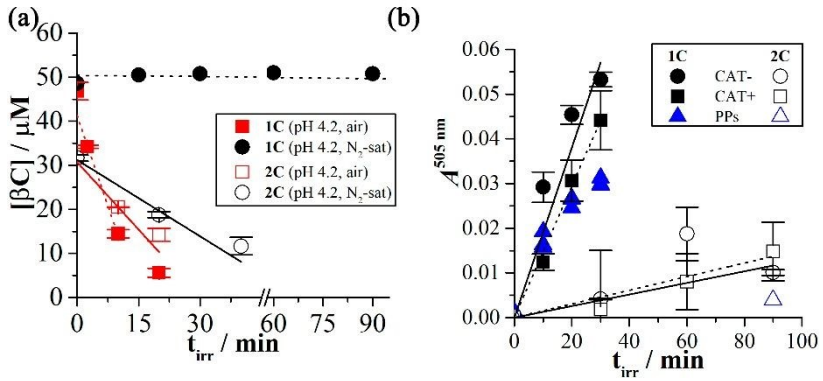

Figure 1. (a) Evolution of **1C** (solid symbols) and **2C** (empty symbols) concentration in air-equilibrated (red squares) and N_2-sat (black circles) acidic (pH 4.2) aqueous solutions as a function of the irradiation time with R-350. Concentrations were assessed using HPLC method described in the experimental section. **(b)** Evolution of the absorbance at 505nm (A^{505nm}) in irradiated solutions as a function of irradiation time with R-350, obtained with the colorimetric reaction from irradiated samples pre-treated (squares) and untreated (circles) with catalase. Up-triangles depict A^{505nm} of the irradiated βC solution at the same dilution to represent the intrinsic contribution of the photoproducts (PPs) to the overall absorbance recorded for the colorimetric method.

UV-visible spectroscopic analysis

The evolution of the photochemical reactions performed in both air-equilibrated and N_2-sat conditions were also monitored by UV-vis absorption spectroscopy (**Figure 2**). In the presence of oxygen, compound **1C** show a spectroscopic degradation pattern with isosbestic points at 210 nm, 231 nm, 263 nm, 301 nm and 371 nm (**Figure 2a**, *left column*) In the case of compound **2C**, the spectroscopic evolution shows pseudo-isosbestic points at 223 nm, 264 nm, 314 nm, 342 nm and 429 nm due to an increase on the absorbance at ~ 325 nm with the concomitant decrease of the main absorption band centered at ~ 370 nm (**Figure 2**, *left column*). To further evaluate the pH effect, **1C** and **2C** samples were irradiated under three additional pH conditions: 5.0, 6.0 and 7.0 (*i.e.*, below the corresponding pK_a values). In both cases, data obtained were qualitatively and quantitatively practically the same within the experimental error (see NED_{tirr} spectra and kinetic traces in **Figures SI.1** and **SI.2**). The latter fact suggests that, in the pH range investigated (4.2 – 6.0), the type and extent of photoproducts formed are the same. Only a distinctive pattern was observed in the case of **2C** at pH 7.0 that will be discussed below (**Figure SI.2(a)**).

Experiments performed under N_2-sat conditions confirm the absence of reaction in the case of **1C**, whereas the apparent consumption of **2C** showed a lower rate compared with that measured by HPLC. This result suggests that the photoproducts formed under these experimental conditions contribute to total absorption in the same region as the reactant **2C** (see below). Interestingly, for **2C**, the pattern of the spectroscopic changes differs from air-equilibrated to N_2-sat irradiated solutions. This is more evident when analyzing the normalized experimental difference (NED_{tirr}) spectra depicted in **Figure 2** (*right column*).

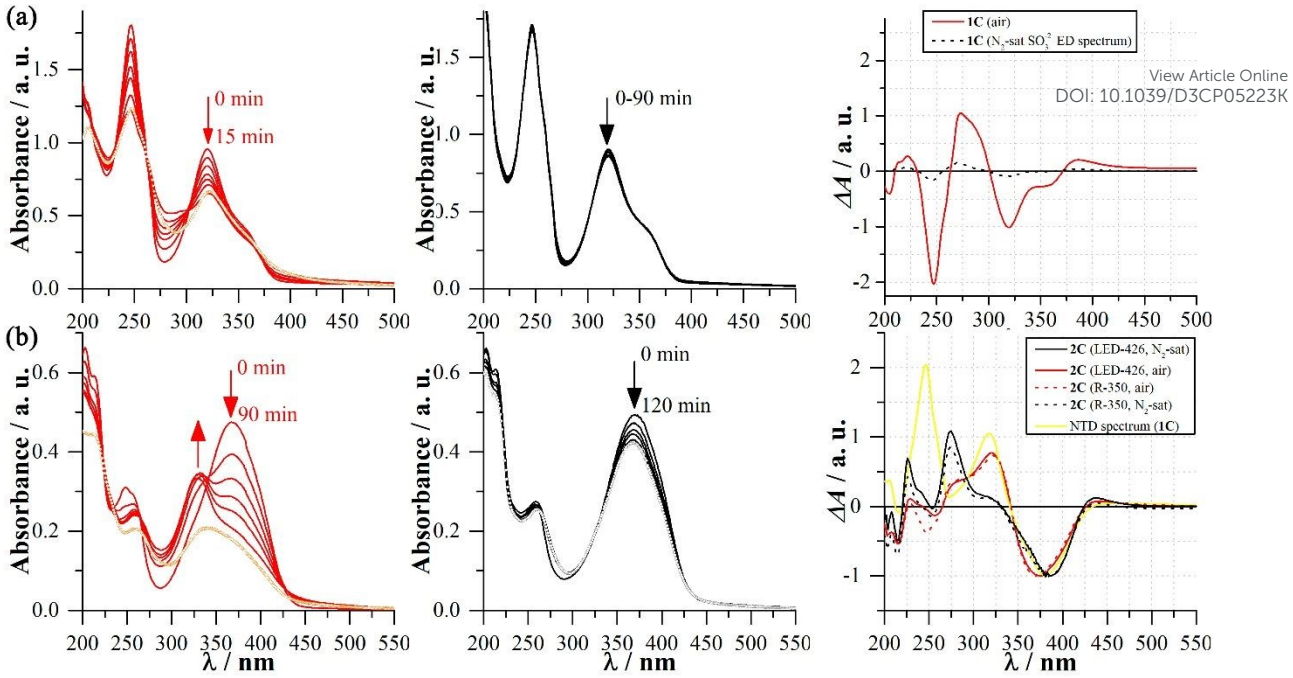

Figure 2. Evolution of the UV-vis absorption spectra of acidic (pH 4.2) aqueous solution of **(a) 1C** (47 μM) and **(b) 2C** (30 μM) under air-equilibrated (*left column*) and N_2-sat (*middle column*) atmospheric conditions, recorded as a function of the irradiation time with R-350. Measurements were made using quartz cells of 1 cm optical path lengths. Single spectra depicted in Orange and grey were recorded from **1C** and **2C** irradiated solutions, respectively, stored in the dark during 26 h. *Right column* depicts the corresponding NED_{tirr} spectra calculated by subtracting the spectra obtained at the maximum irradiation time and the spectra recorded at time cero. For comparative reasons, the so-called Normalized Theoretical Difference (NTD) spectrum (calculated by subtracting the spectra of **1C** and **2C** and depicted in yellow) as well as NED_{tirr} spectra obtained for **2C** irradiated under acidic (pH 4.2), using two different excitation sources (R-350 and LED-426) under two different atmospheric conditions (air-equilibrated and N_2-sat) as depicted in the figure legend are included. Sodium sulfite (Na_2SO_3) was also added as scavenger of molecular oxygen to improve the anaerobic conditions.

In a recent study involving harmaline, a related DHβC compound, it was observed that upon photoexcitation under a nitrogen-saturated atmosphere, the pyridine ring undergoes aromatization, resulting in the production of harmine.[8] To qualitatively investigate a similar mechanism with compound **2C**, we compared the NED_{tirr} spectra corresponding to the experiments performed under N_2-sat atmosphere with the normalized theoretical difference (NTD spectrum). The NTD spectrum was calculated assuming complete conversion of the reagent **2C** into photoproduct **1C** (yellow spectrum in **Figure 2(b)**, *right column*). Interestingly, the evolution of the spectra observed under N_2-sat atmosphere (red dashed line in **Figure 2(b)**, *right column*) exhibits changes in two specific regions of the spectrum, *i.e.*, 225-275 nm and 300-350 nm, with the appearance of shoulders at 241 nm and 318 nm, respectively. Note that the shoulders are close to the absorption maxima exhibited by the NTD spectrum of **1C** formation depicted in yellow. These results suggest that, although not in a significant extent, a **1C**-like photoproduct would be formed and/or accumulated upon photoexcitation of **2C** N_2-sat solutions. This fact is further discussed in the next sections.

The experiments outlined in the preceding paragraphs were conducted using the UVA lamp (R-350) showing a broad emission spectrum (*i.e.*, ~330-370 nm). Within the latter range of the electromagnetic spectrum, both investigated compounds **1C** and **2C** show significant molar

absorption coefficients. Therefore, the photochemical degradation of **2C** can lead to the formation of photoproducts (including **1C**) that can potentially absorb the UVA incident light. This secondary photochemical reaction could be the responsible in preventing the accumulation of **1C**. With this in mind, we performed irradiations of **2C** using a LED-426 as an alternative excitation source (**Figure SI.3**). With this excitation source we aimed at selectively photoexcite **2C** over **1C** and any other photoproducts with absorption maxima in the UVA, to minimize any potential impact on the primary photoproducts. Results showed that under both atmospheric conditions the pattern of the spectral changes was like the pattern observed upon UVA light irradiation (R-350) (**Figure SI.4**). Only a mild difference was observed in the experiment performed under air-equilibrated conditions in the ~250 nm region of the spectra that could be a consequence of a secondary photochemical reactions induced by UVA. Interestingly, the evolution of the spectra observed under N_2-sat atmosphere with both excitation sources (LED-426 and R-350) was similar. Thus, if some **1C**-like photoproduct is formed, this reaction would not represent the main pathway for **2C** photodegradation (see below).

Fluorescence spectroscopic analysis

The evolution of the photochemical reactions under all the investigated experimental conditions were also monitored by excitation-emission fluorescence spectroscopy. As representative examples, **Figure 3** depicts EEMs recorded at the initial (t = 0 min) and maximum irradiation time corresponding to the experiments performed in air-equilibrated and N_2-sat acidic (pH 4.2) solutions of compounds **1** and **2**. The complete set of EEMs (*i.e.*, all irradiation times) recorded for all the photochemical tests performed under diverse experimental conditions (*i.e.*, different pH, excitation wavelengths and oxygen partial pressure) are provided as supplementary information (**Figures SI.5** to **SI.9**). These data confirm the HPLC, and UV-vis absorption spectroscopic results discussed above. Briefly, compound **1C** only shows photodegradation in the presence of oxygen (**Figures 3(a)**, **3(b)**, **SI.5**, and **SI.6**), whereas compound **2C** shows photochemical degradation under both atmospheres investigated (**Figures 3(c) 3(d)**, **SI.7** and **SI.8**). In the latter case, the rate of **2C** consumption observed under N_2-sat conditions was lower than that recorded in air-equilibrated solutions, in line with the results obtained by HPLC. Note that, under N_2-sat conditions, **1C**-like photoproduct formation was not observed, even when the excitation source used was LED-426 (**Figures SI.9**). These results suggest that the photoproduct formed under N_2-sat, although it shows a similar absorption pattern than **1C**, it is a different non-fluorescent structure. In addition, as it was observed by UV-visible spectroscopy, irradiation of compounds **1C** and **2C** under different pH values (pH 5.0, 6.0 and 7.0) showed no qualitative difference on the EEMs profile (**Figures SI.5** and **SI.7**, respectively), confirming the fact that, in the pH range investigated (4.2 – 6.0), the type and extent of photoproducts formed is independent on the proton concentration.

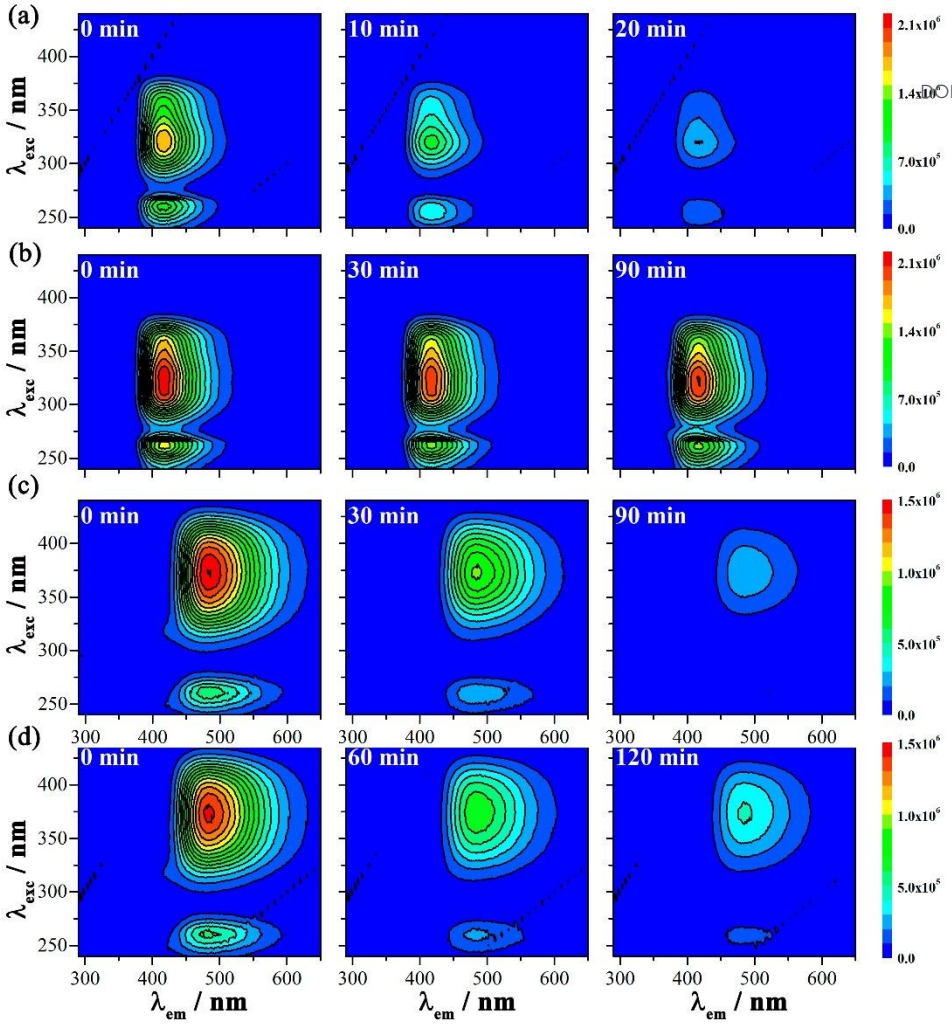

Figure 3. (a) y **(b)** EEMs of **1C** acidic (pH 4.2) solutions irradiated (R-350) under air-equilibrated and N_2-sat conditions. **(c)** y **(d)** EEMs of **2C** acidic (pH 4.2) solutions irradiated (R-350) under air-equilibrated and N_2-sat conditions.

Photoinduced production of hydrogen peroxide

βCs, including compounds **1** and **2** are quite photoactive endogenous compounds [37] with moderate to low efficiency of singlet oxygen production (Φ_Δ = 0.2 and 0.02, for compounds **1C** and **2C**, respectively). [28,36] Upon photoexcitation (with R-350 lamp), hydrogen peroxide (H_2O_2) was also reported to be produced for a few βC derivatives. Typically, the quantum yields of H_2O_2 production (Φ_{H2O2}) reported in the case of other related full aromatic βCs ranged from 10^{-2} to 10^{-3}, and H_2O_2 formation was reported to be associated to the βC photooxidative degradation pathways.[8,30,32,33,36] On the contrary, Φ_{H2O2} value reported for the only 3,4-dihydro-βC investigated to date (*i.e.*, harmaline) was null.[8] However, the production of H_2O_2 by photoexcited compounds **1C** and **2C** remain unknown.

To further investigate this, H_2O_2 formation upon photoexcitation of **1C** and **2C** was quantified herein by using the colorimetric assay described in the methodological section. The H_2O_2 quantification test performed on the irradiated samples shows a clear absorbance increase with time in the peak wavelength of the colorimetric complex (**Figure 1(b)**). To further differentiate if the latter observations correspond to H_2O_2 formation or to the absorption of the photoproducts (up-triangles in **Figure 1(b)**), irradiated samples were treated with catalase prior to the incubation with the

colorimetric reactants. Results showed no significant differences with the untreated samples, indicating that neither **1C** nor **2C** produces a significant amount of H_2O_2 when subject to irradiation. Therefore, the increase in the absorbance at ~500 nm is mainly ascribed to the photoproduct's formation (see below).

Data reported herein represent a unique pattern for these two βCs investigated. Despite the relatively high quantum yield of consumption of these two compounds ($\Phi_R \sim 10^{-2}$) compared to the other βCs previously reported, the lack of H_2O_2 production (see numerical support as supplementary information) suggests that compounds **1C** and **2C** would follow distinctive photochemical pathways, where dissolved molecular oxygen would not play a role as an electron acceptor, for the typical electron transfer reaction reported for other related photoexcited βCs.[32,33,36]

Thermal stability of the photoproducts formed after elapsed irradiations of 1C and 2C

When irradiated solutions of **1C** and **2C** (with ~50-80% of photoconversion) were kept in the dark, a distinctive behavior was observed. Briefly, N_2-sat solutions were stable (grey spectra in **Figure 2**, *middle column*), whereas air-equilibrated solutions showed spectroscopic changes (orange spectra in **Figure 2**, *left column*). The latter fact represents a unique behavior among all the other βCs investigated to date.[8,33,36] Thus, the hydroxy group placed at C(7) of the main βC ring plays a key role. Under the studied experimental conditions, the full spectral evolution of this *thermal reaction* occurs in a somewhat larger timescale than the photochemical reaction (**Figure 4**). The latter reaction could involve intramolecular rearrangements where the solvent could also play a role (see below). The pattern and extent of changes observed were the same in the entire pH range investigated, except for pH 7.0 that is further discussed in the framework of the chemometric analysis described below (see UV-visible spectral evolution, NED_{ter} spectra and kinetics in **Figures SI.10** and **SI.11**). In the case of compound **2C**, the effect of the excitation wavelength on the spectroscopic evolution pattern of the thermal reaction was also explored using LED-426 as excitation source during the pre-irradiation stage (**Figure SI.12**). Results showed a similar trend to that observed upon R-350 excitation, suggesting that secondary photochemical processes are of negligible importance under UVA excitation.

To assess the dependency of the thermal rearrangement reaction of the photoproducts on the presence of molecular oxygen, solutions of **2C** irradiated (R-350 nm) under air-equilibrated conditions were subsequently purged with nitrogen (N_2-sat) and stored in the dark. UV-visible spectra reveal that under these conditions, a thermal reaction continues to occur, showing profiles of spectral changes practically identical to those of the thermal reaction occurring under an air-equilibrated atmosphere (**Figure SI.13(a)**). This is more evident when comparing the NED_{ter} spectra (*i.e.*, solid gray and orange dashed spectra, respectively, in **Figure SI.13(b)**). This suggests that molecular oxygen would not play any significant role in the thermal rearrangement reaction.

View Article Online
DOI: 10.1039/D3CP05223K

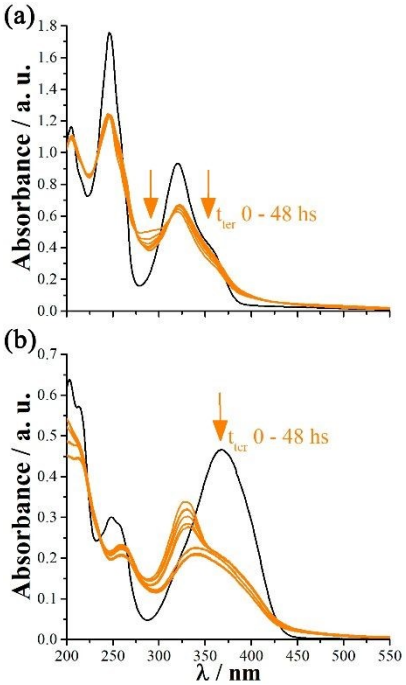

Figure 4. (a) and **(b)** Evolution of the UV-visible absorption spectra (orange) for the thermal reactions of acidic (pH 4.2) aqueous solution of **(a) 1C** (50 μM) and **(b) 2C** (30 μM). Samples were irradiated (R-350) during 60 min and then kept in the dark. For comparative purpose, black lines representing the absorption spectra of non-irradiated **1C** and **2C** solutions are included.

MCR-ALS analysis

In the previous sections, due to the complex photochemistry of **1C** and **2C** combined with the chemical instability of the photoproducts, only a qualitative analysis of the spectral evolution was assessed. To obtain quantitative information as well as the spectroscopic profiles of the species involved in these complex systems, experimental data were further analyzed by MCR-ALS. To this aim, UV-visible spectra for the photochemical and thermal reactions performed under all experimental conditions investigated herein (*i.e.*, two atmospheric conditions and under four different pHs), were used to create column-wise augmented matrices for **1C** and **2C.** Due to the latter augmentation strategy (*i.e.*, concentration mode), the resolved spectra for each compound are common to all experiments. Although the data from both photochemical and thermal reactions were analyzed together, results are depicted separately for clarity.

*Photochemical reaction of **1C***

MCR-ALS analysis of the UV-visible spectroscopic results recorded for irradiated solutions of **1C** revealed that four contributions (denoted hereinafter as F1, F2, F3, and F4) were necessary to properly describe the augmented data matrix. **Figures 5(a)** and **SI.14** displays the spectroscopic profiles of each contribution and their kinetics traces. F1 was attributed to compound **1C** due to its characteristic absorption spectrum with bands centered at 246, 320 and 346 nm, in addition to its kinetic of consumption observed across all pHs. F2 displayed absorption bands at 234, 272, 284, 329 and ~ 380(sh) nm and a much weaker band at ~ 510 nm. It was assigned to one or more products resulting from the primary steps of **1C** photodegradation, as its growth was coupled to **1C** decay during early reaction stages. F3, with absorption bands centered at 249 and 325 nm, emerged after significant F2 accumulation, likely corresponding to a F2 degradation product. The results clearly show that F2 yields F3 through thermal pathways. However, as F2 absorption at 350 (± 15) nm (R-

View Article Online
DOI: 10.1039/D3CP05223K

350) is non-negligible, for irradiated systems the photochemical conversion of F2 to F3 should not be disregarded. F4, with absorption bands at 234, 249, 320 and ~ 420(sh) nm, only appeared at pH 7.0 and it correlates well with the disappearance of F3. Thus, the spectroscopic profiles of F3 and F4 could represent two acid-base species since the timescale of F4 production at pH 7.0 is similar to that of F3 under acidic conditions. Moreover, irradiation at pH 4.2, followed by alkalization to pH 8.5 after irradiation, increased F4 contribution (**Figure SI.16**). Similarly, samples irradiated at pH 7.0 showed an increase in F4 followed by a strong decrease upon acidification below pH 6.3.

Chemometric analysis aligned with NED_{tirr} observations, which indicated qualitatively similar reactions in the pH range, except at pH 7.0, where the relative absorption at ~ 450 nm increased. Notably, the results obtained for pH 4.2 irradiation under N_2-sat conditions and in the presence of Na_2SO_3 as oxygen scavenger (**Figure SI.14**) may be primarily explained by the contribution of F1 (associated with **1C**). Briefly, concentration profiles exhibited minor or null changes (over significantly longer times compared to other conditions), confirming the negligible photochemical reaction in this setup.

*Photochemical reaction of **2C***

In the case of **2C**, MCR-ALS algorithm, applied to the column-wise augmented matrix (i.e. concentration mode) with the non-negativity constraint for both modes (*C* y *S*), resolved three major contributions (denoted as F1, F2, and F3) to the total absorbance (**Figure 5(b)**, *left column*). F1 was assigned to **2C** due to its spectroscopic profile (absorption maxima at 250 and 370 nm) and the concentration decrease as a function of the irradiation time. The increases in the relative concentrations observed for F2 (absorption maxima at 268, 327 and 403(sh)) suggest that this contribution corresponds to a photoproduct formed upon photoexcitation. The third contribution, F3 with absorption maxima at 260 and 351 nm, could be the product of the thermal reaction. Note that both spectral profiles show the low energy absorption band ~350-450 nm. This is typical for the βC-ring suggesting that the photoproducts conserve, to some extent, the pyrido-indole-like structure. Complementary studies performed under other pH conditions (5.0, 6.0 and 7.0) showed similar results (**Figure SI.15**).

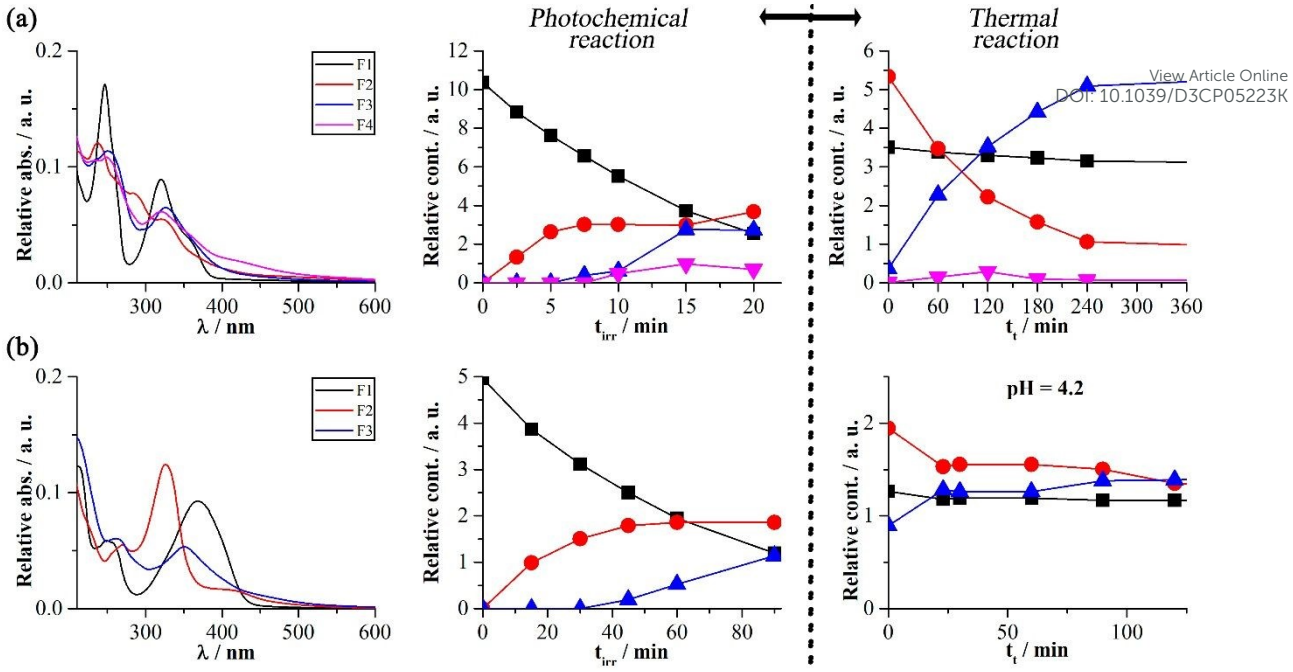

Figure 5. (a) and **(b)** MCR-ALS analysis of the evolution of UV-visible absorption spectra of **1C** and **2C**, respectively, acidic (pH 4.2) solutions irradiated (R-350) under different atmospheric conditions (unimodality and non-negativity restrictions). *Left column*: Spectroscopic profiles of factors F1 – F4. *Middle and right columns:* kinetics of the factors observed for the photochemical and thermal reactions, respectively, observed under air-equilibrated conditions.

*Thermal reaction of the photoproducts of **1C** and **2C***

Regarding the thermal reactions, it stands out that the contributions that explain the experimental trends were the same as those obtained for the photochemical reactions for each compound, respectively. However, their relative contributions varied with respect to storage time in the dark. The thermal reaction that undergo the photoproducts of **1C** (**Figure 5 (a)**, *right column*) shows an increase in the relative contribution of F3 during storage, which in turn correlates with a decay of that corresponding to F2. This trend was observed in all the pH conditions tested (**Figure SI.17**). This would imply that F3 would form from the thermal decomposition of F2. It should be noted that F1, assigned to **1C**, remained constant during dark storage at all pHs tested, implying that **1C** does not undergo a significant thermal reaction. On the other hand, F4 had a significant contribution only in the pH 7.0 and this behavior was correlated with a decrease in the relative contribution of F3. This, as discussed above, could be due to both contributions corresponding to an acid-base pair.

The analysis of the thermal reaction of **2C** shows, within the analyzed time range, negligible changes for F1 contribution assigned to the reagent **2C** (**Figure 5 (b)**, *right column*). On the other hand, the relative contributions of F3 increase with storage time as F2 contributions decrease, reaching constant values after approximately four hours. This trend was observed in all the pH conditions tested (**Figure SI.17**).

PARAFAC analysis

To extract more information from the EEMs discussed above, the PARAFAC algorithm was applied to the collected fluorescence data sets. As previously stated, this analysis allows isolating the spectroscopic profiles of an EEM and its evolution with respect to some variable, this variable being the irradiation time for this specific case.

*Photochemical reaction of **1C***

In the case of **1C**, the algorithm was able to separate two factors that properly explain the experimental data. **Figure 6 (a)** shows their spectroscopic profiles, along with the evolution of their relative fluorescence intensities as a function of irradiation time in an air-equilibrated solution. The first factor has the characteristic excitation and emission spectrum of **1C**. Additionally, it is observed that in both conditions studied the emission of **1C** decreases as the irradiation time increases. Regarding the rate of consumption, similar values were observed for both conditions. F2 factor shows excitation maxima at 280 and ~335 nm, and emission maxima at ~396 nm. This factor contributes very little to the total emission of the solution, but its emission increases as the irradiation progresses. It should be noted that the excitation maxima of this contribution match with those resulting from the MCR-ALS analysis of UV-visible spectroscopy (F2 in **Figure 5(a)**). However, other observed absorption maxima were not detected by analyzing the excitation spectra. Thus, the contribution obtained by MCR-ALS could correspond to more than one chemical species, but just one of them with detectable fluorescence properties.

*Photochemical reaction of **2C***

Similar experiments were performed for **2C** solutions under both atmospheric conditions (**Figure 6 (b)**). In this case, the PARAFAC algorithm was able to explain the emission data using two factors. The first factor corresponds to **2C** due to its excitation and emission spectroscopic characteristics. **2C** is consumed with similar rates under both conditions studied. On the other hand, considering the excitation and emission profiles obtained, the extremely weak signal associated with the second factor was assigned to the presence of traces of **1C** in the commercial standard of **2C**. Similarly to what was mentioned for the **1C** reaction, **2C** exhibits a faster photodegradation in air-equilibrated conditions than in the N_2-sat atmosphere, and the latter seems to decrease its consumption rate at long irradiation times. Regarding the reaction under N_2-sat conditions, the discrepancies between the results obtained by UV-visible absorption measurements and fluorescence spectroscopy were previously mentioned. It should be noted that in this aspect the PARAFAC algorithm managed to obtain the kinetic profile of **2C** consumption despite the high degree of overlap of its UV-visible spectrum with that of other species/s present in the reaction mixture.

View Article Online
DOI: 10.1039/D3CP05223K

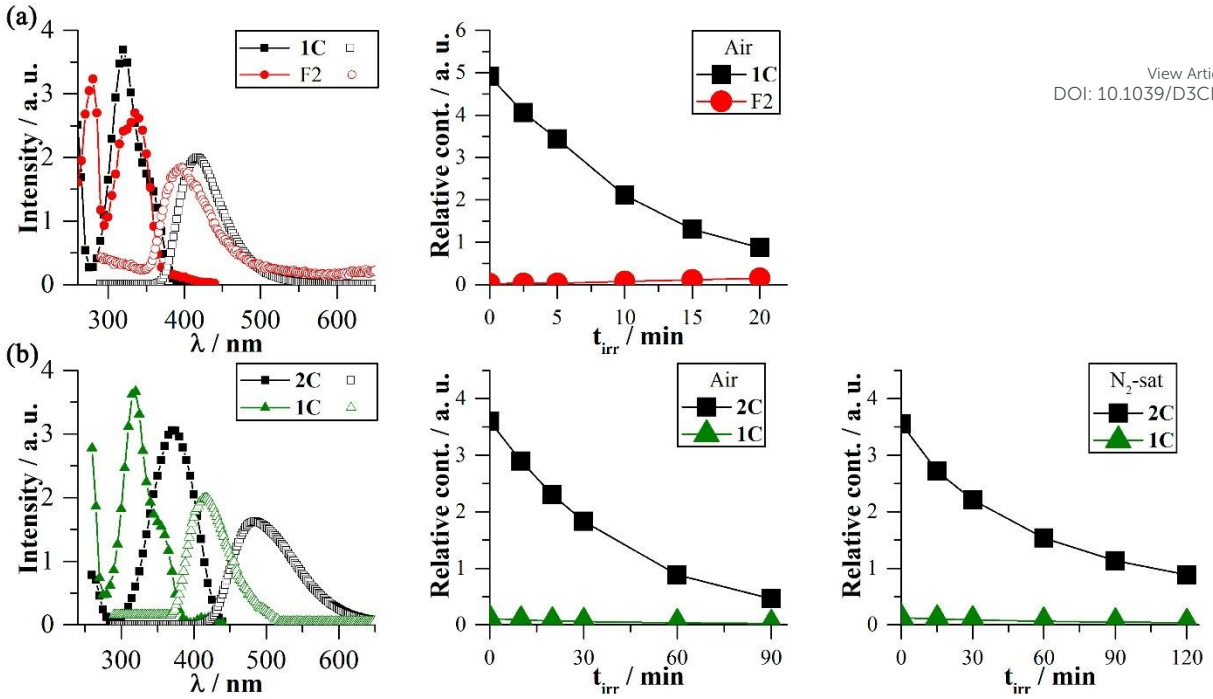

Figure 6. (a) and **(b)** PARAFAC analysis of the evolution of EEMs of **1C** and **2C**, respectively, acidic (pH 4.2) irradiated (R-350) under different atmospheric conditions. *Left column*: Spectroscopic profiles of factors **1C**, **2C** and F2. Excitation spectra (solid symbols) and emission spectra (empty symbols). *Middle and right columns:* kinetics of the factors observed for the photochemical reactions studied.

HRESI-Mass spectrometry analysis

To characterize the photoproducts, acidic solutions of **1C** and **2C** were irradiated (R-350 and/or LED-426, pH 4.2) under air-equilibrated and N_2-sat atmospheric conditions and kept in the dark for more than 48 h. High-resolution mass spectrometry (HRMS) with electrospray ionization (ESI) was employed for analysis. Unlike harmaline findings,[8] good signal-to-noise ratio were challenging for **1C** and **2C**, possibly due to the hydroxyl substituent present at C(7), affecting βC nucleus basicity and, therefore, the protonation of gaseous molecules to form the molecular ions [M+H]. Nevertheless, the high sensitivity of the ESI-MS (Orbitrap) equipment used herein enable reliable results.

In the case of air-equilibrated **1C** irradiated (R-350) solutions, although a clear decrease (consumption) on the molecular ion signal of **1C** was observed as a function of the irradiation time, hardly any photoproduct ionizable at ESI was detected under our experimental conditions. On the contrary, in the case of **2C** solutions, irradiations carried out under air-equilibrated solutions showed a clear decrease in the relative signal with m/z = 201 (assigned to **2C**, **Figure SI.18**) with the concomitant appearance of products with m/z = 217 compatible with [**2C**+O]+H, as well as other two signals with m/z = 233 and 251 compatible with [**2C**+2O]+H and [**2C**+2OH+O]+H, respectively. Considering these m/z values and both photochemical and thermal reactions associated with indolic compounds of the DHβC type, plausible structures were tentatively assigned for the stable photoproducts under the HRMS-ESI-MS analysis conditions (**Figure 7 (a)** and **(b)**).

Unlike harmaline (*i.e.*, a related 3,4-dihydro-βC), ESI spectra of N_2-sat solutions of **2C**, irradiated with both R-350 and LED-426, showed no photoproducts in the m/z range from 100 to 800 (**Figure 7 (c)** and **(d)**). Moreover, the intensity of **2C**, relative to the **1C** signal, showed no significant changes within the first 90 min of irradiation (**Figure SI.18**). Considering the actual decrease in the **2C** concentration (i.e., overall fluorescence intensity) observed by HPLC and PARAFAC analysis (see above), ESI results suggest the formation of an isomer. According to the chemical nature of the reactant, a quinone-like (**Q**) structure can be proposed (**Scheme 2**). To further investigate this hypothesis, the electronic structure of **Q** was studied by DFT and TD-DFT calculations and compared to that of **C**. The geometry of **Q** at its ground electronic state was optimized by DFT and the vertical transition energies were calculated at the optimized ground-state geometry by TD-DFT. **Figure SI.19** compare the calculated absorption spectral features of **Q** with respect to those of **C**. Noteworthy, in the spectral region between 300 and 600 nm, the calculated absorption spectra of both **2C** and **2Q** show one intense electronic transition at $\lambda \sim 350$ nm and a less intense electronic transition at lower energy which is displaced to the red in **2Q** ($\lambda_{calc} = 447$ nm) relative to **2C** ($\lambda_{calc} = 405$ nm). The calculated electronic spectrum of **1C** shows only one intense electronic transition at $\lambda_{calc} = 330$ nm. On the other hand, the calculated spectrum of **1Q** shows two electronic transitions, one at $\lambda_{calc} = 370$ nm and a less intense one at $\lambda_{calc} = 479$ nm. The SCF energies of **Q** species are always higher than those of **C** species. The SCF energy difference between **Q** and **C** species ($\Delta(E^Q - E^C)$, is ~ 30 Kcal mol^{-1} and ~56 Kcal mol^{-1} for compounds **2** and **1**, respectively. Therefore, **2Q** species is more stable than **1Q** species, relative to the **C** species, by ~26 Kcal mol^{-1}. The similarities between the position of the calculated electronic transitions of **2C** and **2Q** suggests the small or negligible spectral changes shown in the UV-vis spectra (**Figure 2**). Under air-equilibrated conditions, quinone-like structures would be susceptible for reaction with dissolved molecular oxygen giving rise to the formation of oxidative photoproducts (**Scheme 2**). These hypotheses need to be further investigated.

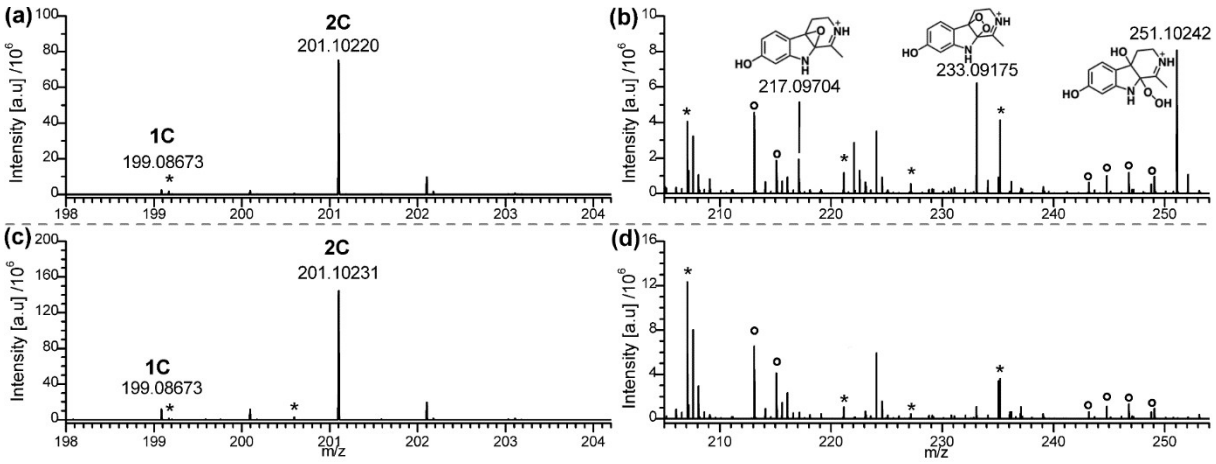

Figure 7. Mass spectra, recorded on positive ion mode, corresponding to irradiated (60 min, R-350) acidic (pH4.2) solution of **2C** under air-equilibrated (**(a)** and **(b)**) and N_2-sat (**(c)** and **(d)**) atmospheres. Chemical structure and the corresponding exact mass of the photoproducts formed are depicted close to the corresponding peak. White symbols and asterisks depict solvent clusters and other background signals.

CONCLUSIONS

βC alkaloids are photoactive compounds, with promising pharmacological properties. Therefore, understanding their photochemical behavior is crucial. Relative high levels of harmol (**1C**) and harmalol (**2C**) were found in key light-exposed biological environments/organs, including plant aerial organs, eye crystalline, and melanocytes. We hereby present, for the first time, the photochemical behavior of harmol (**1C**) and harmalol (**2C**) in water under different experimental conditions. This study aims to further assess the impact of pH, oxygen partial pressure, and excitation wavelength on the extent and profile of photodegradation. Based on the experimental data presented herein, a reaction mechanism was suggested (**Scheme 2**) and the following main conclusions and considerations were achieved:

- ✓ The full aromatic derivative studied, compound **1C**, only displays photochemical reaction in the presence of molecular oxygen, as it was observed for harmine, [8] another structural related βC.
- ✓ Interestingly, **2C** (3,4-dihydro-βC or DHβC) shows photochemical reactivity under both atmospheres, and as it was reported for its methoxylated structural analogue (harmaline), [8] the partial pressure of O_2 also modulates the reaction rate and the photooxidation profile.
- ✓ In the presence of dissolved molecular oxygen, irradiated solutions of **1C** and **2C** lead to the formation of unstable photoproducts, exhibiting further thermal (non-photochemical) reactions. This behavior is markedly distinctive compared to other βCs and DHβCs derivatives studied to date.
- ✓ In contrast to the reported behavior of harmaline, the formation of the full aromatic derivative **1C** when **2C** is subject to irradiation in the absence of O_2 was not detected. On the contrary, ESI-MS analysis suggest the formation of a structural isomer derived from **2C**. Theoretical calculations may suggest that quinone-like (**Q**) structure could be formed.
- ✓ The photochemical and thermal reactions studied in this article proved to be complex in terms of the number of contributing species and their high degree of spectra overlap. However, MCR-ALS of UV-visible absorption spectra allowed the isolation of spectral profiles associated with individual contributions. Additionally, the construction of expanded matrices in *C-mode* allowed the resolution of concentration profiles for the different tested conditions, leading to the identification of an acid-base equilibrium between two products. Finally, the high selectivity and sensitivity of fluorescence spectroscopy, combined with the decomposition of recorded EEMs using the PARAFAC algorithm, allowed for the extraction of highly precise concentration profiles. This is particularly evident in the photochemical reaction of **2C** under N_2-sat conditions. Briefly, the apparent masking of conversion degree

of the reactant due to the overlap of its UV-visible absorption spectrum with those of the photoproducts (particularly, **Q**) was resolved through the multivariate analysis of EEMs.

- ✓ Regarding the biological implications of the findings reported herein, it was demonstrated that **2C** does not produce hydrogen peroxide upon photoexcitation. This results in connection with the already published null capability of singlet oxygen formation and low DNA-nucleobase photooxidative damage, and supports the hypothesis of using compound **2** for the pharmacological treatment of hypopigmentation related disorders (*e.g.*, vitiligo) previously suggested.[22]

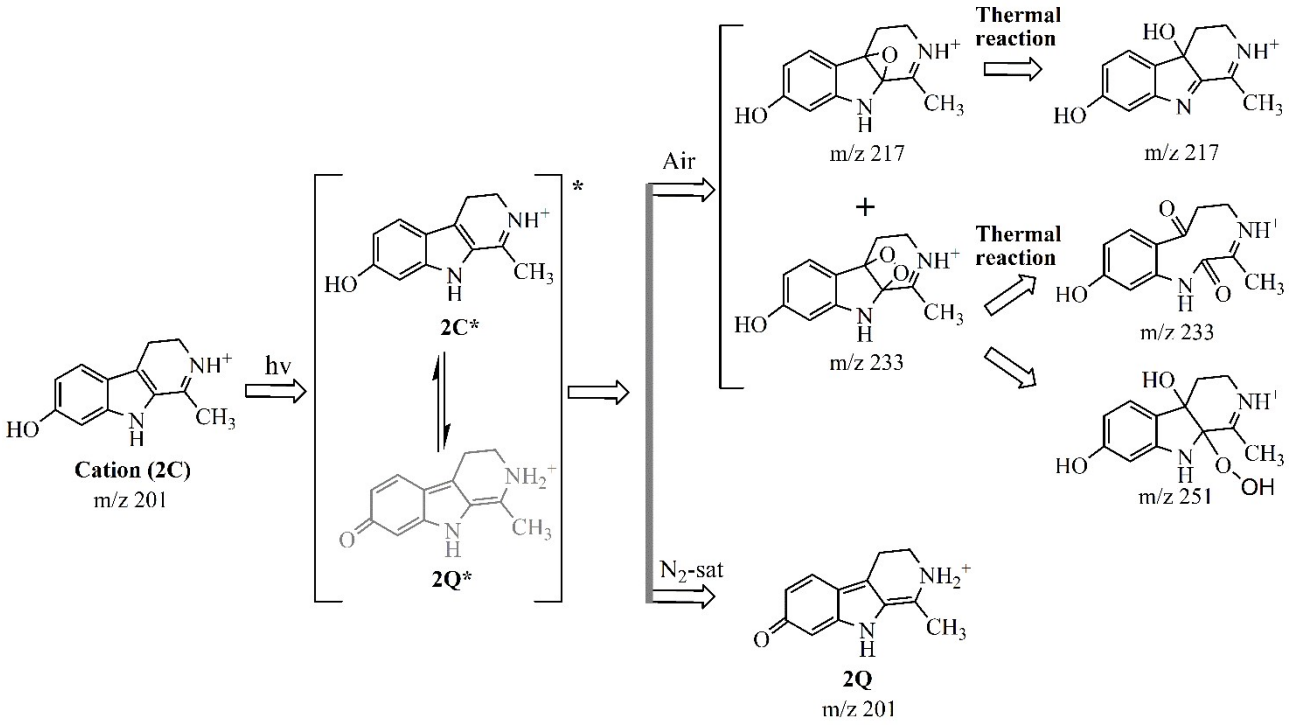

Scheme 2. Photochemical and thermal rearrangement proposed for the photodegradation of **2C** alkaloid in aqueous solution (pH 4.2), under the two different atmospheres investigated (air-equilibrated and N_2-sat).

ACKNOWLEDGEMENTS

The present work was partially supported by ANPCyT (PICT 2018-03193 and 2021-00044). MPD, REB, EW, FSGE and FMC are research members of CONICET. TSL and FDV thank CONICET for their doctoral and postdoctoral fellowships, respectively.

REFERENCES

1 M. S. Siderhurst, D. M. James, C. D. Rithner, D. L. Dick and L. B. Bjostad, *J. Econ. Entomol.*, 2005, **98**, 1669–1678.
2 U. Breyer-Pfaff, G. Wiatr, I. Stevens, H. Jörg Gaertner, G. Mundle and K. Mann, *Life Sci.*, 1996, **58**, 1425–1432.
3 T. Zhao, S. S. Zheng, B. F. Zhang, Y. Y. Li, S. W. A. Bligh, C. H. Wang and Z. T. Wang, *Food Chem.*, **134**, 1096–1105.
4 M. W. Machado, C. S. Neto, J. Salgado, G. Zaffari, A. Barison, F. R. Campos, Y. E. de Corilo, M. N. Eberlin and M. W. Biavatti, *Brazilian Arch. Biol. Technol.*, **53**, 901–910.
5 T. Herraiz, D. González, C. Ancín-Azpilicueta, V. J. Arán and H. Guillén, *Food Chem. Toxicol.*, 2010, **48**, 839–845.
6 B. Ospina-Calvo, E. De Gerónimo, F. D. Villarruel, V. C. Aparicio, L. Ashworth, R. Erra-Balsells and F. M. Cabrerizo, *Photochem. Photobiol.*, , DOI:https://doi.org/10.1111/php.13837.
7 J. Stöckigt, A. P. Antonchick, F. Wu and H. Waldmann, *Angew. Chemie Int. Ed.*, 2011, **50**, 8538–8564.
8 F. Villarruel, M. P. Denofrio, F. A. O. Rasse-Suriani, F. S. García Einschlag, T. Schmidt De León, R. Erra-Balsells and F. M. Cabrerizo, *J. Photochem. Photobiol. B Biol.*, 2019, **199**, 111600.

9 M. Kartal, M. L. Altun and S. Kurucu, *J. Pharm. Biomed. Anal.*, 2003, **31**, 263–269.
10 A. Movafeghi, M. Abedini, F. Fathiazad, M. Aliasgharpour and Y. Omidi, *Nat. Prod. Res.*, 2009, **23**, 301–308.
11 R. Cao, W. Peng, Z. Wang and A. Xu, *Curr. Med. Chem.*, 2007, **14**, 479–500.
12 T. Akabli, F. Lamchouri, S. Senhaji and H. Toufik, *Struct. Chem.*, 2019, **30**, 1495–1504.
13 M. A. M. El Gendy, A. A. Soshilov, M. S. Denison and A. O. S. El-Kadi, *Food Chem. Toxicol.*, 2012, **50**, 353–362.
14 S. Sarkar, P. Bhattacharjee, T. Ghosh and K. Bhadra, *Futur. J. Pharm. Sci.*, , DOI:10.1186/s43094-020-00045-x.
15 G. M. Olmedo, L. Cerioni, M. M. González, F. M. Cabrerizo, V. A. Rapisarda and S. I. Volentini, *Food Microbiol.*, 2017, **62**, 9–14.
16 G. M. Olmedo, L. Cerioni, M. M. González, F. M. Cabrerizo, S. I. Volentini and V. A. Rapisarda, *Front. Microbiol.*, , DOI:10.3389/fmicb.2017.00347.
17 M. L. Alomar, F. A. Rasse-Suriani, A. Ganuza, V. M. Coceres, F. M. Cabrerizo and S. O. Angel, *BMC Res Notes*, 2013, **6**, 193.
18 M. L. Alomar, J. G. Yañuk, S. O. Angel, M. M. Gonzalez and F. M. Cabrerizo, *Front. Microbiol.*, , DOI:10.3389/fmicb.2021.716534.
19 D. J. Moura, M. F. Richter, J. M. Boeira, J. A. Pêgas Henriques and J. Saffi, *Mutagenesis*, 2007, **22**, 293–302.
20 Y. H. Tse, I. Mak and B. F. Dickens, *Biochem. Pharmacol.*, 1991, **42**, 459–464.
21 S. Senhaji, F. Lamchouri, T. Akabli and H. Toufik, *Struct. Chem.*, 2022, 883–895.
22 S.-Y. Park, Y.-H. Kim, Y.-H. Kim, G.-T. Park and S.-J. Lee, *BMB Rep.*, 2010, **43**, 824–829.
23 M. C. Biondic and R. Erra-Balsells, *J. Chem. Soc. Perkin Trans. 2*, 1993, 887–903.
24 M. C. Biondic and R. Erra-Balsells, *J. Photochem. Photobiol. A Chem.*, 1990, **51**, 341–353.
25 M. C. Biondic and R. Erra-Balsells, *J. Chem. Soc. Perkin Trans. 2*, 1997, 1323–1328.
26 G. Serdaroğlu, *Res. Chem. Intermed.*, 2020, **46**, 961–982.
27 M. V. Cañamares, F. Pozzi and J. R. Lombardi, *J. Phys. Chem. C*, 2019, **123**, 9262–9271.
28 F. D. Villarruel, M. P. Denofrio, R. Erra-Balsells, E. Wolcan and F. M. Cabrerizo, *Phys. Chem. Chem. Phys.*, 2020, **22**, 20901–20913.
29 J. G. Yañuk, M. P. Denofrio, F. A. O. Rasse-Suriani, F. D. Villarruel, F. Fassetta, F. S. García Einschlag, R. Erra-Balsells, B. Epe and F. M. Cabrerizo, *Org. Biomol. Chem.*, 2018, **16**, 2170–2184.
30 F. A. O. Rasse-Suriani, F. S. García-Einschlag, M. Rafti, T. Schmidt De León, P. M. David Gara, R. Erra-Balsells and F. M. Cabrerizo, *Photochem. Photobiol.*, 2018, **94**, 36–51.
31 B. Hemmateenejad, A. Abbaspour, H. Maghami, R. Miri and M. R. Panjehshahin, *Anal. Chim. Acta*, 2006, **575**, 290–299.
32 F. A. O. Rasse-Suriani, M. Paula Denofrio, J. G. Yañuk, M. Micaela Gonzalez, E. Wolcan, M. Seifermann, R. Erra-Balsells and F. M. Cabrerizo, *Phys. Chem. Chem. Phys.*, 2016, **18**, 886–900.
33 M. M. Gonzalez, M. L. Salum, Y. Gholipour, F. M. Cabrerizo and R. Erra-Balsells, *Photochem. Photobiol. Sci.*, 2009, **8**, 1139–1149.
34 F. M. Cabrerizo, M. L. Dantola, A. H. Thomas, C. Lorente, A. M. Braun, E. Oliveros and A. L. Capparelli, *Chem. Biodivers.*, 2004, **1**, 1800–1811.
35 M. P. Denofrio, F. D. Villarruel, R. Erra-Balsells, P. R. Ogilby, E. Wolcan and F. M. Cabrerizo, *Phys. Chem. Chem. Phys.*, 2021, **23**, 11039–11051.
36 M. M. Gonzalez, J. Arnbjerg, M. Paula Denofrio, R. Erra-Balsells, P. R. Ogilby and F. M. Cabrerizo, *J. Phys. Chem. A*, 2009, **113**, 6648–6656.
37 M. P. Denofrio, J. M. Paredes, J. G. Yañuk, M. D. Giron, R. Salto, E. M. Talavera, L. Crovetto and F. M. Cabrerizo, *Photochem. Photobiol. Sci.*, 2023, **22**, 487–501.